MICROSCOPY

Microscopy, 2021, 171–177
doi:10.1093/jmicro/dfaa075
Advance Access Publication Date: 15 December 2020

Review

Local structure analysis of amorphous materials by angstrom-beam electron diffraction

Akihiko Hirata*

Department of Materials Science, Waseda University, Shinjuku, Tokyo 169-8555, Japan; Kagami Memorial Research Institute for Materials Science and Technology, Waseda University, Shinjuku, Tokyo 169-0051, Japan; WPI Advanced Institute for Materials Research, Tohoku University, Sendai, Miyagi 980-8577, Japan and Mathematics for Advanced Materials-OIL, AIST, Sendai, Miyagi 980-8577, Japan

*To whom correspondence should be addressed. E-mail: ahirata@aoni.waseda.jp

Received 23 September 2020; Editorial Decision 10 December 2020; Accepted 14 December 2020

Abstract

The structure analysis of amorphous materials still leaves much room for improvement. Owing to the lack of translational or rotational symmetry of amorphous materials, it is important to develop a different approach from that used for crystals for the structure analysis of amorphous materials. Here, the angstrom-beam electron diffraction method was used to obtain the local structure information of amorphous materials at a sub-nanometre scale. In addition, we discussed the relationship between the global and local diffraction intensities of amorphous structures, and verified the effectiveness of the proposed method through basic diffraction simulations. Finally, some applications of the proposed method to structural and functional amorphous materials are summarized.

Key words: electron diffraction, amorphous materials, local structures, STEM

Introduction

The demand for the local structure analysis of amorphous materials has increased with an increase in its industrial applications. The structural details of amorphous materials obtained from the local structure analysis are important for improving the properties or functions of amorphous materials, just like in crystals. However, some fundamental issues limit the in-depth understanding of the atomic configurations of amorphous materials because of their lack of translational or rotational symmetry. Generally, amorphous structures are analysed using a pair distribution function (PDF) based on X-ray or neutron diffraction experiments [1–3]. The PDF analysis provides information on the average interatomic bond length and coordination number. Recently, the structural factors of amorphous materials have been obtained over a wide scattering angle range using synchrotron radiation, leading to a high-resolution PDF [4]. However, the PDF analysis cannot adequately unravel the individual local structures in amorphous structures, although the overall statistical information can be obtained accurately. Therefore, it is important to develop a new method with a higher 'spatial' resolution compared to that of PDF to directly obtain local information on the structures of amorphous materials.

Transmission electron microscopy (TEM) has been utilized for the observation of amorphous materials because of its high spatial resolution. In the 1970s and 1980s, high-resolution electron microscopy (HREM) was utilized for the direct observation of amorphous materials [5–7]. The HREM images give a maze-like contrast, which is typical of amorphous structures and includes the noise and structural information. Krivanek *et al.* [5] reported that the local structural order embedded in the noise becomes observable when the size of the amorphous material is >1.5 nm. Hirotsu *et al.* systematically combined HREM and computational simulations and reported the optimum defocus conditions for the imaging of the local structural order embedded in amorphous structures [8–10]. They reported the existence of a local crystal-like structural order, especially in the metal-metalloid-type amorphous alloys. In the 2000s, the quality of the HREM images of amorphous structures was drastically improved using aberration-corrected TEM [11,12].

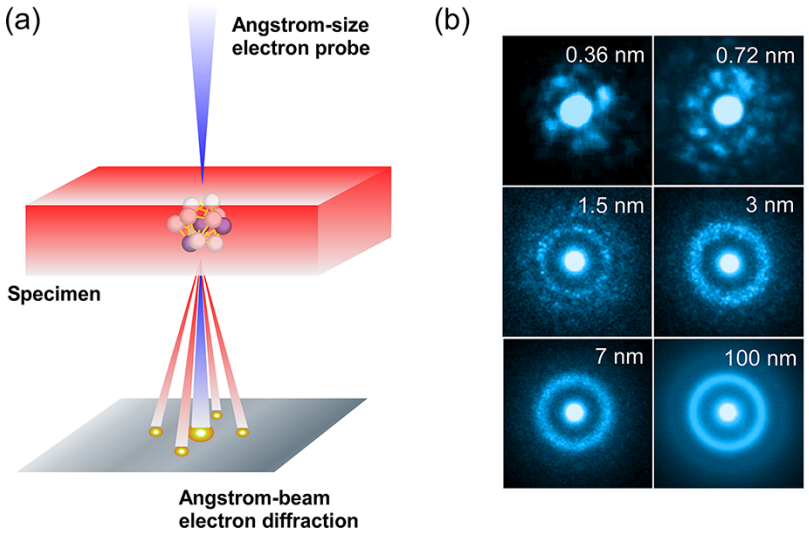

Fig. 1. (a) Schematic diagram of the angstrom-beam electron diffraction method. (b) Electron diffraction patterns obtained from amorphous Zr-Ni alloy with different beam sizes. The pattern with 100-nm beam size shows typical halo rings, indicating that the region includes atoms that allow the use of isotropic assumption. The continuous halo rings gradually become discrete with decreasing beam size (reproduced from [22]).

Yamasaki *et al*. reported the depth-resolution imaging of amorphous films using aberration-corrected TEM [13]. Additionally, fluctuation microscopy has also been reported as an effective approach for statistically detecting the medium range order of amorphous structures [14,15].

Meanwhile, a focussed electron beam generated by a field emission–type gun has been utilized in TEM/scanning transmission electron microscopy (STEM) to obtain local diffraction patterns from the local sub-nanoscale regions of amorphous materials. The method is generally referred to as micro- or nano-beam electron diffraction. Although this method was actively performed for crystals by Cowley *et al*. in the 1970s and 1980s [16,17], there are only few reports on the application of this method to amorphous materials in the early stage [9,18]. The observation of the non-crystalline order in metallic glasses by nano-beam electron diffraction was introduced in the late 2000s [19–21].

Global and local diffraction of amorphous materials

In this section, we discuss the marked differences between the global and local diffraction intensities obtained from amorphous materials [1]. Considering their disordered nature, the global diffraction intensity of amorphous structures should be spatially isotropic. Generally, halo rings (Fig. 1b) are constantly observed from the relatively wide areas of amorphous materials, even when the sample is moved or rotated during TEM. This implies that its diffraction intensity is isotropic in the three-dimensional reciprocal space and therefore can be reduced to a one-dimensional radial profile. For monatomic systems, the three-dimensional intensity is written as follows:

$$I(\boldsymbol{Q}) = \sum_{m=1}^{N} f_m^2(\boldsymbol{Q}) + \sum_{m=1}^{N} \sum_{\substack{n=1 \\ (n\neq m)}}^{N} f_m(\boldsymbol{Q}) f_n(\boldsymbol{Q}) e^{i\boldsymbol{Q}\cdot\boldsymbol{r}_{mn}}, \quad (1)$$

where $\boldsymbol{Q}$ is the scattering vector ($|\boldsymbol{Q}| = 4\pi sin\theta/\lambda$), f_n is the atomic scattering factor for the n^{th} atom and $\boldsymbol{r}_n$ is the positional vector for the n^{th} atom. Eq. (1) can be transformed into a one-dimensional representation using a polar coordinate as follows:

$$I(Q) = Nf^2(Q) + Nf^2(Q) \int_0^{\infty} 4\pi r^2 (\rho(r) - \rho_0) \frac{sinQr}{Qr} dr, \quad (2)$$

where ρ_0 is the average atom number density and $\rho(r)$ is the radial number density function. In contrast to the diffraction patterns of crystals, where discrete diffraction spots are formed in a three-dimensional reciprocal space, it is unnecessary to consider the three-dimensional information of amorphous materials for its global diffraction intensities. However, the local diffraction intensities of amorphous materials are discrete and spotty shaped. This is because the local structures usually contain only a few dozen atoms, in which the isotropic assumption is no longer valid. Consequently, Eq. (1) is used rather than Eq. (2). In summary, the diffraction patterns of the local structures of amorphous materials are composed of spotty discrete intensity regions rather than halo patterns. It is important to note that the discrete diffraction patterns of the local structures of amorphous materials do not imply crystal structures. In the next section, we demonstrate a method to obtain symmetric diffraction patterns with relatively sharp diffraction spots of the non-crystalline local structures of amorphous materials.

Angstrom-beam electron diffraction experiment

Based on the above diffraction theory, for the angstrom-beam electron diffraction experiment, we considered the realistic local diffraction patterns of metallic glasses. Fig. 1a is the schematic illustration of the angstrom-beam electron diffraction experiment, and Fig. 1b shows the diffraction patterns with several beam sizes obtained from the metallic glass [22]. When the beam size was reduced to 0.36 nm, the diffraction pattern with spotty crystal-like intensity was observed. Note that the local structures did not have a crystalline order, but exhibited non-crystalline features. The non-crystalline local structures do not possess any rotational symmetries, as opposed to the normal crystals. Such non-crystalline local structures can be obtained from the glassy structure models made by molecular dynamics (MD) simulations.

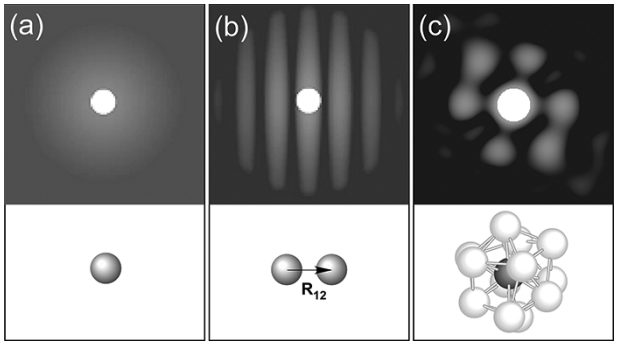

Fig. 2. Simulated diffraction patterns obtained from (a) single Au atom, (b) paired Au atoms and (c) atomic cluster extracted from the Zr-Pt metallic glass model. Atomic configurations corresponding to the patterns are also shown at the bottom.

Figure 2 illustrates the electron diffraction patterns simulated from typical atomic clusters as well as those simulated from a single atom and paired atoms. The simulated pattern from a single atom (Fig. 2a) exhibited featureless intensity, which is equivalent to the square of the atomic scattering factor. In contrast, in the diffraction patterns simulated from the paired atoms (Fig. 2b), variations were observed in the diffraction intensity along the direction parallel to the vector $\mathbf{R}_{12}$, which originated from a correlation term in Eq. (1). In addition, as shown in the diffraction pattern simulated from the atomic cluster in Fig. 2c, the intensity distribution was strongly dependent on the direction in the three-dimensional space and had a similar appearance to the diffraction spots normally observed in crystals, although the intensity was blurred. As mentioned above, atomic clusters in metallic glasses are normally extracted from the MD structure models through the Voronoi polyhedral analysis [23]. It should be noted that the Voronoi indices assigned to each atomic cluster indicate rough geometric features.

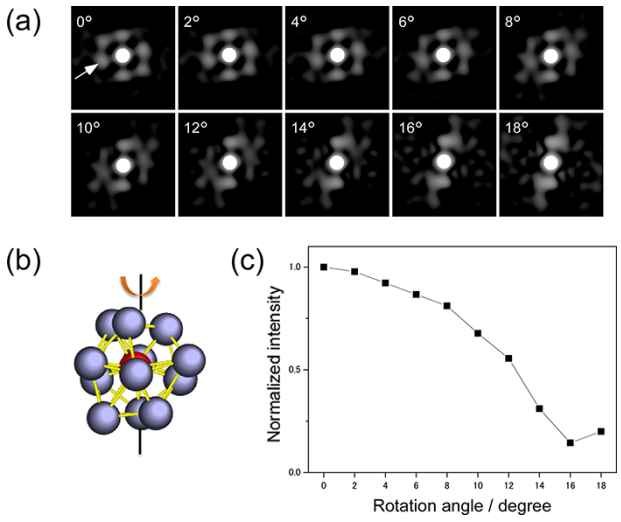

Fig. 3. (a) Sequential change in the simulated diffraction patterns when rotating the atomic cluster shown in (b). (b) Atomic cluster extracted from the Zr-Pt metallic glass model as well as its rotation axis. (c) Change in the diffraction intensity for the spot indicated by arrow in (a).

The spatial feature of the diffraction intensity can be examined in a three-dimensional reciprocal space by rotating the atomic cluster [24]. Fig. 3a illustrates a series of simulated diffraction patterns corresponding to different cluster orientations. As shown in Fig. 3b, while a pair of diffraction spots was maintained in an axis, the other pairs of diffraction spots faded away, as usually observed in crystals. The change in the diffraction intensity indicated by the arrow in Fig. 3a is shown in Fig. 3c. As shown in Fig. 3c, the intensity of the diffraction spot is strongly dependent on the cluster orientation. This implies that the diffraction intensity from the cluster

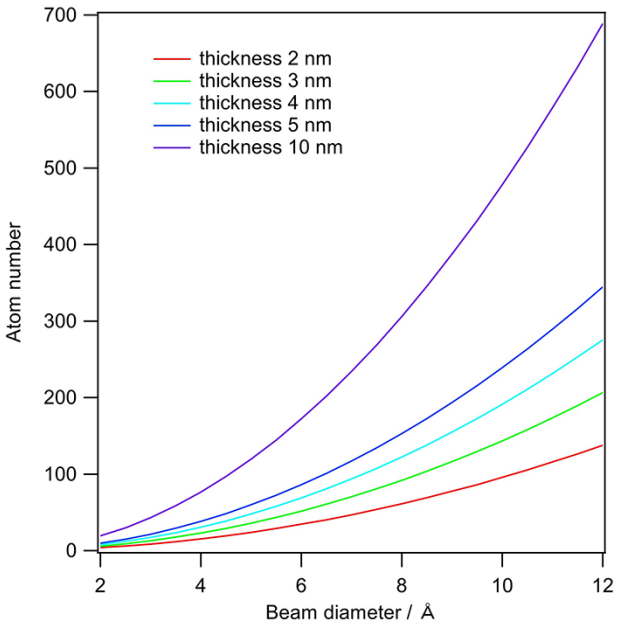

Fig. 4. Plots for the atom numbers in the columns that allow the passage of electron beams with changes in the beam diameter of the electron probe. The sample thicknesses used in the calculation are 2, 3, 4, 5 and 10 nm.

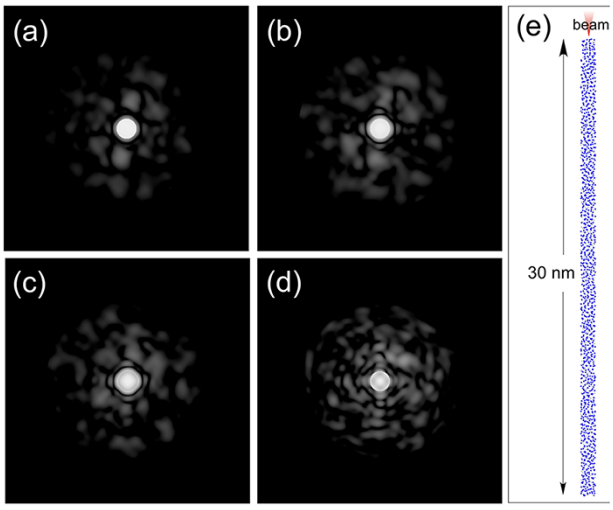

Fig. 5. Thickness effects on the diffraction patterns of the amorphous materials. The multislice calculations were performed for the structure models of the Zr-Pt metallic glass with thicknesses of (a) 2.5, (b) 5.0, (c) 10.0 and (d) 30.0 nm. The structure model used for the pattern (d) with 30.0-nm thickness is also depicted in (e).

is discretized in reciprocal space, even though the cluster does not exhibit any crystalline features.

The samples used for TEM analysis should be sufficiently thin to allow the passage of electrons, but should also be thicker than the size of the atomic cluster. Therefore, it is necessary to consider the effect of the sample thickness on the diffraction intensity. Here, we roughly estimated the atom numbers in the column of metallic glass samples through which electrons pass. Fig. 4 plots the atom numbers in the columns for several thicknesses, assuming that the average diameter of atoms and packing density were 0.28 nm and 0.7, respectively. Note that 0.7 is the approximate average packing density value for typical metallic glasses. When the beam diameter was <4 Å, the atom number was less than 100, even at a thickness of 10 nm. In addition, in this range, the sample thickness had no significant effect on the atom number. However, with an increase in the beam diameter, the thickness significantly affected the atom number in the column. The smaller beam size is critical to suppress the rise in the atom number. Hence, this method is called the 'angstrom-beam' electron diffraction.

The effect of the sample thickness on the atom number in real situations can be confirmed by the multislice calculation for large-scale MD simulation models. It is important to note that the multislice calculation is a simulation method for diffractions or images that allow for the plural scattering effect. Fig. 5 displays the calculated electron diffraction patterns of the Zr-Pt MD models with different sample thicknesses. Note that the thinner model is always a part of the thicker model. The diffraction patterns from the 2.5- and 5-nm thickness models exhibited relatively strong paired diffraction spots similar to those from the individual atomic cluster (Fig. 1b). At a thickness of 10 nm, the paired diffraction spots were still observed; however, the intensity becomes non-symmetric. Interestingly, the overall feature of the pattern of the 10-nm thickness model was not very different from that of the 2.5-nm thickness model. These results indicate that a thickness of <10 nm (possibly <5 nm) is the minimum requirement for the direct observation of the atomic cluster by the angstrom-beam electron diffraction method. At a thickness of 30 nm, the diffraction pattern still exhibited a spotty intensity rather than halo rings; however, the background became much stronger.

To understand the spatial extension of the local structures in amorphous materials, the scanning function of STEM was utilized to obtain diffraction mappings [24,25]. Based on the STEM results, we discussed the correlation length, spatial distribution and structural details of the medium-range order of the metallic glass. Fig. 6 demonstrates an example of the angstrom-beam electron diffraction mapping of the PdCuNiP bulk metallic glass. Over 1000 diffraction patterns were sequentially acquired from a thin area of 6×6 nm^2 of the sample using the STEM mode. Each diffraction pattern was recorded based on the information on the positions in the real space. As shown in Fig. 6b, the diffraction mapping was reconstructed using the recorded data after the experiment. When the mapping was reconstructed using a certain diffraction vector (inset of Fig. 6b), the brighter regions with a size of ∼1.0–1.5 nm were widely distributed in the mapping. Fig. 6c illustrates a series of diffraction patterns obtained from the region surrounded by a white lines.

The angstrom-beam electron diffraction patterns were interpreted by calculating the diffraction patterns for the reference structure models (atomic configurations) obtained from the MD simulations. The interatomic potentials should be considered when calculating the structures by the MD simulations. A direct modelling method should be used when the potentials are absent. In addition, the validity of the potentials should be confirmed, even if present. To meet these requirements, a local reverse Monte Carlo (local RMC) simulation dedicated to angstrom-beam electron diffraction has been recently proposed [26] as shown in Fig. 7. The procedure of the local RMC is similar to that of the conventional RMC simulation [27], where atoms are moved randomly to fit the experimental data. The

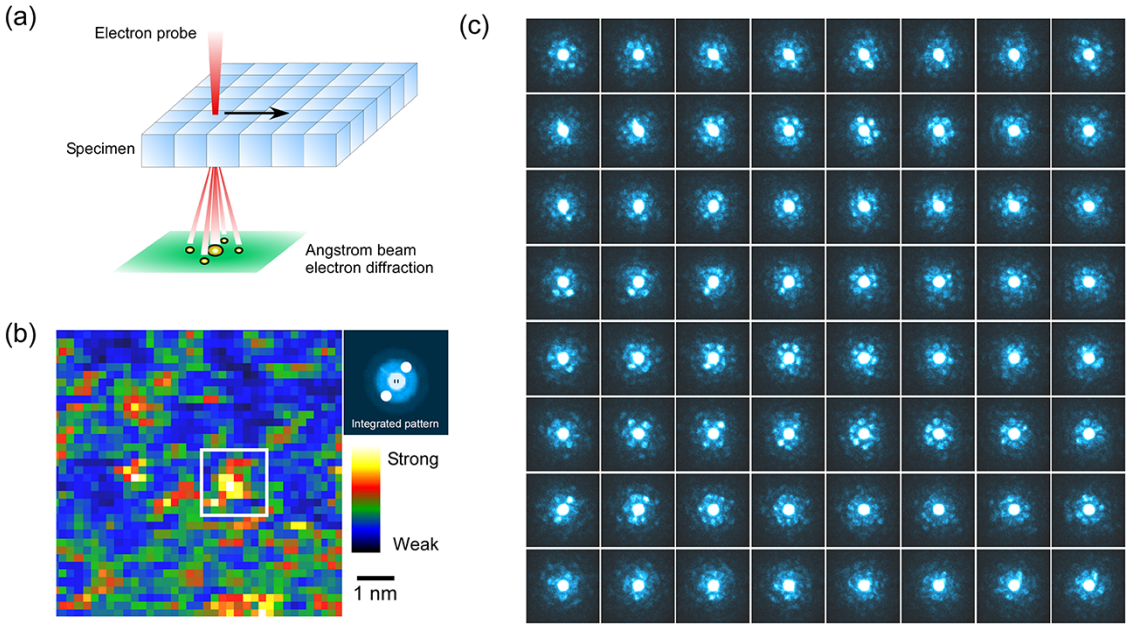

Fig. 6. (a) Schematic diagram of the angstrom-beam electron diffraction mapping. (b) Diffraction map constructed using the paired white circles in the integrated pattern shown in the inset. (c) Diffraction patterns obtained from each dot in the area surrounded by the white lines in (b). (Reproduced from [24]).

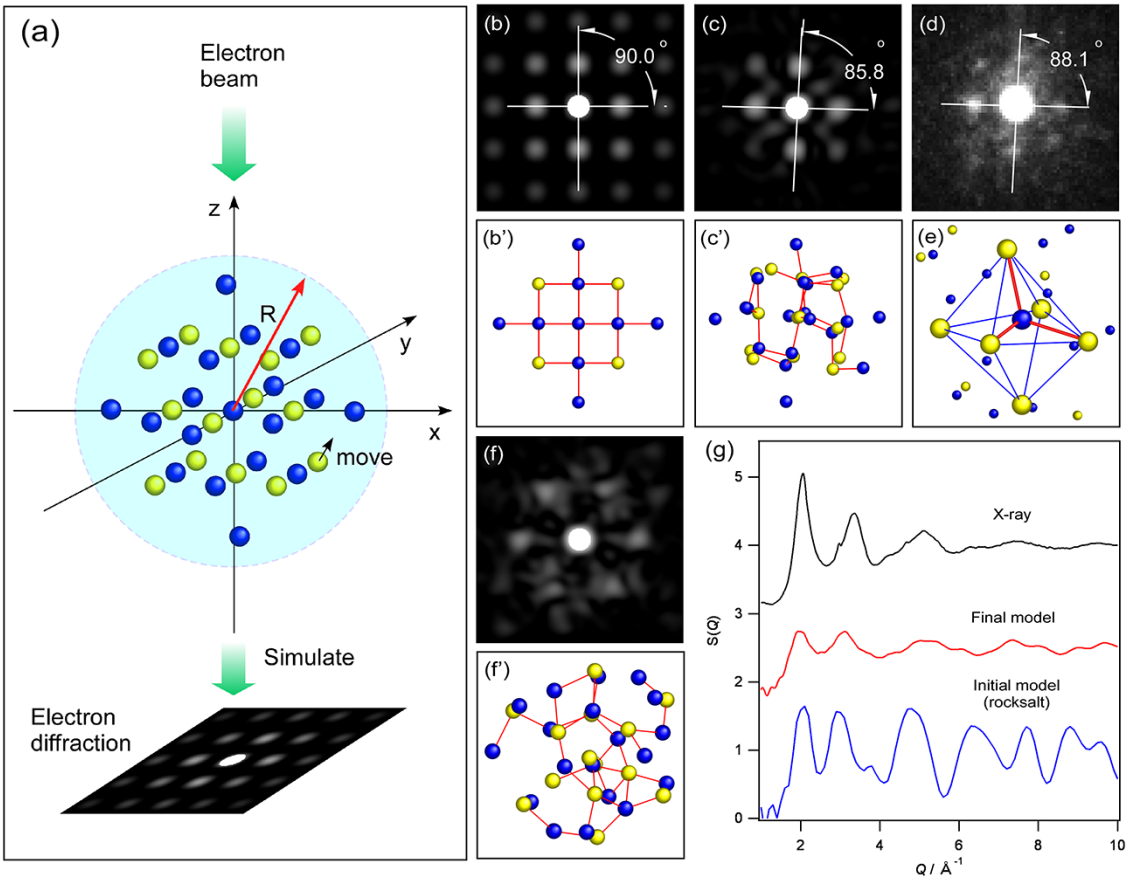

Fig. 7. Analysis of the amorphous Ge-Sb-Te (phase-change recording material) [26]. (a) Schematic diagram of the local RMC procedure. The local RMC simulation started with a NaCl crystal structure as an initial model shown in (b'). The final model of (c') was obtained by moving atoms randomly to fit the experimental pattern of (d). The patterns of (b) and (c) correspond to the models of (b') and (c'), respectively. (e) Distorted octahedron observed in the final model. (f) The model viewed from a different orientation, together with the corresponding simulated diffraction pattern of (f'). (g) Local structure factors for the initial and final models compared with the global structure factor measured by X-ray diffraction. (Reproduced from [26]).

RMC simulation was initially developed to construct structure models for disordered materials based on global diffraction data obtained from the whole area of specimens [27]. Note that the intensity of global diffraction data is written by Eq.(2). Although the RMC software has been improved extensively, the technique was still not applicable to local diffraction data. We have therefore developed the local RMC technique that enables us to perform structure modelling to fit the local experimental data having anisotropic two-dimensional information which can be described by Eq.(1).

Applications for a variety of amorphous materials

The angstrom-beam electron diffraction method has been applied to several amorphous materials. In this section, we review the reported applications revealing local atomic configurations for a variety of structural and functional amorphous materials [22,26,28–32].

Initially, this technique was applied to the short-range order (nearest neighbour environment) of metallic glasses [22,28]. Here, we discuss the physical meaning of the observed short-range order mentioned earlier. In 1952, Frank reported that non-crystalline icosahedron, which has a local energy less than those of the fcc or hcp crystals, should be locally formed in the liquid or supercooled liquid of metals [33]. Inspired by this work, several studies have been conducted to unravel the presence of an icosahedron in liquid, supercooled liquid and glasses. It is well known that the icosahedron cannot densely fill the entire space, unlike the crystalline motifs. This limitation is known as geometric frustration. In this situation, it is important to determine the appearance of the icosahedron in the densely packed glass states. Hence, we observed a Zr-Pt metallic glass, where several icosahedra should form based on the simulations, by the angstrom-beam electron diffraction method [28]. We found that the frequently observed diffraction patterns can be interpreted as a heavily distorted icosahedron rather than a perfect icosahedron. The heavy distortion of each icosahedron presumably addresses the geometric frustration mentioned above.

Amorphous materials may have inhomogeneous or heterogeneous nanostructures rather than perfectly homogeneous nanostructures. For example, the inhomogeneous nanostructure that includes the Si and SiO_2 nanoregions of amorphous monoxide (SiO), which is a candidate for the anode of Li-ion battery, has generated debate among researchers for years. By applying the scanning angstrom-beam electron diffraction technique, we successfully examined the nanoscale inhomogeneity of amorphous materials. In addition, by combining this technique with synchrotron X-ray diffraction, an inhomogeneous structure model that includes the Si and SiO_2 nanoregions with interfacial suboxide parts was proposed,

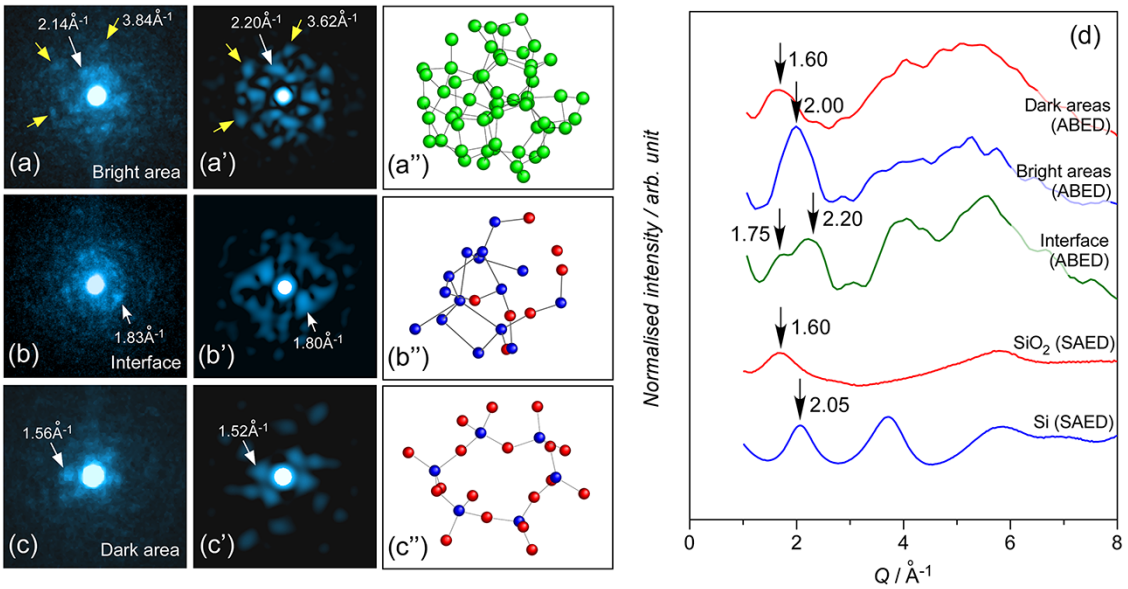

Fig. 8. Analysis of the inhomogeneous amorphous SiO [29]. Angstrom-beam electron diffraction patterns obtained from (a) bright contrast, (b) interface and (c) dark contrast regions in ADF-STEM images. Simulated patterns of (a′), (b′) and (c′), which were simulated from the models of (a″), (b″) and (c″), were consistent with the experimental patterns of (a), (b) and (c), respectively. The intensity profiles constructed by collecting diffraction patterns from several regions with dark contrast, bright contrast and interface regions are shown in (d). (Reproduced from [29]).

as shown in Fig. 8 [29]. It is important to note that a specially designed 3.5-μm condenser aperture leading to a beam diameter of 0.8 nm was used to improve the resolution in the reciprocal space. This work explicitly demonstrates the importance of the local structural information for determining the inhomogeneous amorphous structure that cannot be uniquely identified by the global information such as the X-ray structure factor. In addition, the inhomogeneity of metallic glasses was also revealed by the scanning angstrom-beam electron diffraction method [30].

Consequently, the local structure models based on the angstrom-beam electron diffraction data was constructed using the local RMC modelling method, as previously mentioned. For the phase change recording materials (e.g. $Ge_2Sb_2Te_5$), we applied this technique to build plausible structure models based on the corresponding crystal structure [26]. From the amorphous $Ge_2Sb_2Te_5$, three types of relatively symmetric diffraction patterns were frequently observed, as shown in Fig. 7. Based on this, the local structure models were constructed by the local RMC modelling method, as previously mentioned. The local RMC procedure was initiated from the NaCl-type crystal structure, giving similar diffraction patterns in the experiment rather than a random structure. The heavily distorted NaCl-type structure obtained as a final model is consistent with the angstrom-beam electron diffraction patterns, as well as the global structure factor of X-ray diffraction. It is important to note that the resultant structure model exhibited non-crystalline features, although the symmetry was close to that of the NaCl crystal.

Concluding remarks

To unravel the complicated structures of amorphous materials, the global and local structure information are critical, and both of them should be obtained if possible. This is because the structure model is not unique for a global structure factor or pair distribution function. The angstrom-beam electron diffraction method provided local structure information, owing to its high spatial resolution. This method does not provide an overall picture of amorphous structures, but provides useful insights on the global structure factors. In other words, the global structure models have become interpreted based on the local information. Additionally, combining the scanning function of STEM with this method, the spatial extension and distribution of local structures was determined. For future studies, this method can be conflated with mathematical sciences or informatics to obtain further statistical and meaningful information. For example, a huge amount of diffraction patterns could be automatically classified into several categories using machine learning techniques. If realized, the angstrom-beam electron diffraction method would become a more convenient analytical tool for disordered materials.

Acknowledgements

I would like to thank Professor Mingwei Chen at the Johns Hopkins University for his support.

Funding

This work was partly carried out at the Joint Research Center for Environmentally Conscious Technologies in Materials Science (project no. 31015) at ZAIKEN, Waseda University. This work was also supported by JSPS KAKENHI Grant Number JP20H05881.

References

1. Warren B E (1990) *X-Ray Diffraction* (Dover Publications, New York).
2. Guinier A (1994) *X-Ray Diffraction in Crystals, Imperfect Crystals, and Amorphous Bodies* (Dover Publications, New York).

3. Cusack N E (1987) *The Physics of Structurally Disordered Matter: An Introduction* (CRC Press, Boca Raton).
4. Kohara S, and Suzuya K (2003) High-energy X-ray diffraction studies of disordered materials. *Nucl. Instrum. Methods Phys. Res. B* 199: 23–28.
5. Krivanek O L, Gaskell P H, and Howie A (1976) Seeing order in 'amorphous' materials. *Nature* 262: 454–457.
6. Gaskell P H, and Smith D J (1980) Investigations of the structure of amorphous and partially crystalline metallic alloys by high resolution electron microscopy. *J. Microsc.* 119: 63–72.
7. Ichinose H, and Ishida Y (1983) High resolution electron microscopic observation of the structure and relaxation phenomenon of $Fe_{40}Ni_{40}P_{14}B_6$ amorphous alloy. *Trans. Jpn. Inst. Met.* 24: 405–412.
8. Hirotsu Y, and Akada R (1984) High resolution electron microscopic observation of microcrystalline domains in an amorphous $Fe_{84}B_{16}$ alloy. *Jpn. J. Appl. Phys.* 23: L479–L481.
9. Hirotsu Y, Ohkubo T, and Matsushita M (1998) Study of amorphous alloy structures with medium range atomic ordering. *Microsc. Res. Tech.* 40: 284–312.
10. Ohkubo T, and Hirotsu Y (2003) Electron diffraction and high-resolution electron microscopy study of an amorphous $Pd_{82}Si_{18}$ alloy with nanoscale phase separation. *Phys. Rev. B* 67: 094201.
11. Hirotsu Y, Nieh T G, Hirata A, Ohkubo T, and Tanaka N (2006) Local atomic ordering and nanoscale phase separation in a Pd-Ni-P bulk metallic glass. *Phys. Rev. B* 73: 012205.
12. Hirata A, Hirotsu Y, Nieh T G, Ohkubo T, and Tanaka N (2007) Direct imaging of local atomic ordering in a Pd-Ni-P bulk metallic glass using Cs-corrected transmission electron microscopy. *Ultramicroscopy* 107: 116–123.
13. Yamasaki J, Mori M, Hirata A, Hirotsu Y, and Tanaka N (2015) Depth-resolution imaging of crystalline nanoclusters attached on and embedded in amorphous films using aberration-corrected TEM. *Ultramicroscopy* 151: 224–231.
14. Treacy M M J, and Ribson J M (1996) Variable coherence microscopy: a rich source of structural information from disordered materials. *Acta Cryst. A* 52: 212–220.
15. Voyles P M, and Abelson J R (2003) Medium-range order in amorphous silicon measured by fluctuation electron microscopy. *Sol. Energy Mater. Sol. Cells* 78: 85–113.
16. Cowley J M, and Spence J C H (1979) Innovative imaging and microdiffraction in STEM. *Ultramicroscopy* 3: 433–438.
17. Cowley J M (1985) High-resolution electron microscopy and microdiffraction. *Ultramicroscopy* 18: 11–17.
18. Cowley J M (2002) Electron nanodiffraction methods for measuring medium-range order. *Ultramicroscopy* 90: 197–206.
19. Hirata A, Morino T, Hirotsu Y, Itoh K, and Fukunaga T (2007) Local atomic structure analysis of Zr-Ni and Zr-Cu metallic glasses using electron diffraction. *Mater. Trans.* 48: 1299.
20. Hirata A, Hirotsu Y, Amiya K, Nishiyama N, and Inoue A (2008) Nanocrystallization of complex $Fe_{23}B_6$-type structure in glassy Fe-Co-B-Si-Nb alloy. *Intermetallics* 16: 491–497.
21. Hirata A, Hirotsu Y, Amiya K, and Inoue A (2008) Crystallization process and glass stability of an $Fe_{48}Cr_{15}Mo_{14}C_{15}B_6Tm_2$ bulk metallic glass. *Phys. Rev. B* 78: 144205.
22. Hirata A, Guan P F, Fujita T, Hirotsu Y, Inoue A, Yavari A R, Sakurai T, and Chen M W (2011) Direct observation of local atomic order in a metallic glass. *Nat. Mater* 10: 28–33.
23. Borodin V A (1999) Local atomic arrangements in polytetrahedral materials. *Phil. Mag. A* 79: 1887–1907.
24. Hirata A, and Chen M W (2016) Structure analysis of amorphous materials using a STEM electron diffraction method. *Mater. Jpn.* 55: 8–14.
25. Hirata A, and Chen M W (2014) Angstrom-beam electron diffraction of amorphous materials. *J. Non-Crys. Sol.* 383: 52–58.
26. Hirata A, Ichitsubo T, Guan P F, Fujita T, and Chen M W (2018) Distortion of local atomic structures in amorphous Ge-Sb-Te phase change materials. *Phys. Rev. Lett.* 120: 205502.
27. McGreevy R L (2001) Reverse Monte Carlo modelling. *J. Phys. Condens. Mat.* 13: R877–R913.
28. Hirata A, Kang L J, Fujita T, Klumov B, Matsue K, Kotani M, Yavari A R, and Chen M W (2013) Geometric frustration of icosahedron in metallic glasses. *Science* 341: 376–379.
29. Hirata A, Kohara S, Asada T, Arao M, Yogi C, Imai H, Tan Y W, Fujita T, and Chen M W (2016) Atomic-scale disproportionation in amorphous silicon monoxide. *Nat. Commun.* 7: 11591.
30. Zhu F, Hirata A, Liu P, Song S, Tian Y, Han J, Fujita T, and Chen M (2017) Correlation between local structure order and spatial heterogeneity in a metallic glass. *Phys. Rev. Lett.* 119: 215501.
31. Nishino H, Fujita T, Cuong N T, Tominaka S, Miyauchi M, Iimura S, Hirata A, Umezawa N, Okada S, Nishibori E *et al.* (2017) Formation and characterization of hydrogen boride sheets derived from MgB_2 by cation exchange. *J. Am. Chem. Soc.* 139: 13761–13769.
32. Han A, Hirata A, Du J, Ito Y, Fujita T, Kohara S, Ina T, and Chen M (2018) Intercalation pseudocapacitance of amorphous titanium dioxide@ nanoporous graphene for high-rate and large-capacity energy storage. *Nano Energy* 49: 354–362.
33. Frank F C (1952) Supercooling of liquids. *Proc. R. Soc. A* 215: 43–46.